Research Article | Vol. 25, No. 5 | 6 Mar 2017 | OPTICS EXPRESS 4845

Optics EXPRESS

Hybrid laser written waveguides in fused silica for low loss and polarization independence

JUN GUAN,[1,3] XIANG LIU,[1] PATRICK S. SALTER,[1] AND MARTIN J. BOOTH[1,2,*]

[1]*Department of Engineering Science, University of Oxford, Parks Road, Oxford, OX1 3PJ, UK*
[2]*Centre for Neural Circuits and Behaviour, University of Oxford, Mansfield Road, Oxford, OX1 3SR, UK*
[3]*jun.guan@eng.ox.ac.uk*
[*]*martin.booth@eng.ox.ac.uk*

Abstract: Photonic integrated circuits (PICs) written with an ultrashort pulsed laser provide advantages in a range of applications, such as photon-based quantum information processing, where low insertion loss and low polarization dependence are critical concerns. Here we demonstrate the inscription of hybrid waveguides in fused silica at a pulse repetition rate of 1MHz that fulfill both these criteria. The mechanisms for propagation and coupling losses are identified and decoupled, with separate sections of the waveguide minimizing for each and an adiabatic mode conversion between the two. Moreover, differing sources of birefringence were revealed to be non-parallel for the waveguides, such that structures can be designed where these competing sources cancel to remove any polarization dependence.

OCIS codes: (130.2755) Glass waveguides; (140.3390) Laser materials processing; (250.5300) Photonic integrated circuits; (270.5585) Quantum information and processing.

References and links

1. G. D. Marshall, A. Politi, J. C. F. Matthews, P. Dekker, M. Ams, M. J. Withford, and J. L. O'Brien, "Laser written waveguide photonic quantum circuits," Opt. Express **17**(15), 12546–12554 (2009).
2. L. Sansoni, F. Sciarrino, G. Vallone, P. Mataloni, A. Crespi, R. Ramponi, and R. Osellame, "Polarization entangled state measurement on a chip," Phys. Rev. Lett. **105**(20), 200503 (2010).
3. A. Crespi, R. Ramponi, R. Osellame, L. Sansoni, I. Bongioanni, F. Sciarrino, G. Vallone, and P. Mataloni, "Integrated photonic quantum gates for polarization qubits," Nat. Commun. **2**, 566 (2011).
4. J. O. Owens, M. A. Broome, D. N. Biggerstaff, M. E. Goggin, A. Fedrizzi, T. Linjordet, M. Ams, G. D. Marshall, J. Twamley, M. J. Withford, and A. G. White, "Two-photon quantum walks in an elliptical direct-write waveguide array," New J. Phys. **13**(7), 075003 (2011).
5. T. Meany, M. Delanty, S. Gross, G. D. Marshall, M. J. Steel, and M. J. Withford, "Non-classical interference in integrated 3D multiports," Opt. Express **20**(24), 26895–26905 (2012).
6. A. Crespi, R. Osellame, R. Ramponi, V. Giovannetti, R. Fazio, L. Sansoni, F. De Nicola, F. Sciarrino, and P. Mataloni, "Anderson localization of entangled photons in an integrated quantum walk," Nat. Photonics **7**(4), 322–328 (2013).
7. N. Spagnolo, C. Vitelli, L. Aparo, P. Mataloni, F. Sciarrino, A. Crespi, R. Ramponi, and R. Osellame, "Three-photon bosonic coalescence in an integrated tritter," Nat. Commun. **4**, 1606 (2013).
8. G. Di Giuseppe, L. Martin, A. Perez-Leija, R. Keil, F. Dreisow, S. Nolte, A. Szameit, A. F. Abouraddy, D. N. Christodoulides, and B. E. A. Saleh, "Einstein-Podolsky-Rosen spatial entanglement in ordered and anderson photonic lattices," Phys. Rev. Lett. **110**(15), 150503 (2013).
9. M. Tillmann, B. Dakić, R. Heilmann, S. Nolte, A. Szameit, and P. Walther, "Experimental boson sampling," Nat. Photonics **7**(7), 540–544 (2013).
10. R. Heilmann, R. Keil, M. Gräfe, S. Nolte, and A. Szameit, "Ultraprecise phase manipulation in integrated photonic quantum circuits with generalized directional coupler," Appl. Phys. Lett. **105**(6), 061111 (2014).
11. Z. Chaboyer, T. Meany, L. G. Helt, M. J. Withford, and M. J. Steel, "Tunable quantum interference in a 3D integrated circuit," Sci. Rep. **5**, 9601 (2015).
12. A. Crespi, R. Osellame, L. Sansoni, P. Mataloni, F. Sciarrino, and R. Ramponi, "Fabrication of quantum photonic integrated circuits by means of femtosecond laser pulses," Found. Phys. **44**(8), 843–855 (2014).
13. T. Meany, D. N. Biggerstaff, M. A. Broome, A. Fedrizzi, M. Delanty, M. J. Steel, A. Gilchrist, G. D. Marshall, A. G. White, and M. J. Withford, "Engineering integrated photonics for heralded quantum gates," Sci. Rep. **6**, 25126 (2016).

#283255 https://doi.org/10.1364/OE.25.004845
Journal © 2017 Received 20 Dec 2016; revised 31 Jan 2017; accepted 1 Feb 2017; published 22 Feb 2017

Optics EXPRESS

14. B. J. Smith, D. Kundys, N. Thomas-Peter, P. G. R. Smith, and I. A. Walmsley, "Phase-controlled integrated photonic quantum circuits," Opt. Express **17**(16), 13516–13525 (2009).
15. J. B. Spring, B. J. Metcalf, P. C. Humphreys, W. S. Kolthammer, X. M. Jin, M. Barbieri, A. Datta, N. Thomas-Peter, N. K. Langford, D. Kundys, J. C. Gates, B. J. Smith, P. G. R. Smith, and I. A. Walmsley, "Boson sampling on a photonic chip," Science **339**(6121), 798–801 (2013).
16. B. J. Metcalf, N. Thomas-Peter, J. B. Spring, D. Kundys, M. A. Broome, P. C. Humphreys, X.-M. Jin, M. Barbieri, W. Steven Kolthammer, J. C. Gates, B. J. Smith, N. K. Langford, P. G. R. Smith, and I. A. Walmsley, "Multiphoton quantum interference in a multiport integrated photonic device," Nat. Commun. **4**, 1356 (2013).
17. B. J. Metcalf, J. B. Spring, P. C. Humphreys, N. Thomas-Peter, M. Barbieri, W. S. Kolthammer, X. Jin, N. K. Langford, D. Kundys, J. C. Gates, B. J. Smith, P. G. R. Smith, and I. A. Walmsley, "Quantum teleportation on a photonic chip," Nat. Photonics **8**(10), 770–774 (2014).
18. A. Politi, M. J. Cryan, J. G. Rarity, S. Yu, and J. L. O'Brien, "Silica-on-Silicon waveguide quantum circuits," Science **320**(5876), 646–649 (2008).
19. J. W. Silverstone, R. Santagati, D. Bonneau, M. J. Strain, M. Sorel, J. L. O'Brien, and M. G. Thompson, "Qubit entanglement between ring-resonator photon-pair sources on a silicon chip," Nat. Commun. **6**, 7948 (2015).
20. J. Carolan, C. Harrold, C. Sparrow, E. Martín-López, N. J. Russell, J. W. Silverstone, P. J. Shadbolt, N. Matsuda, M. Oguma, M. Itoh, G. D. Marshall, M. G. Thompson, J. C. F. Matthews, T. Hashimoto, J. L. O'Brien, and A. Laing, "Universal linear optics," Science **349**(6249), 711–716 (2015).
21. L. T. Feng, M. Zhang, Z. Y. Zhou, M. Li, X. Xiong, L. Yu, B. S. Shi, G. P. Guo, D. X. Dai, X. F. Ren, and G. C. Guo, "On-chip coherent conversion of photonic quantum entanglement between different degrees of freedom," Nat. Commun. **7**, 11985 (2016).
22. N. C. Harris, G. R. Steinbrecher, J. Mower, Y. Lahini, M. Prabhu, T. Baehr-Jones, M. Hochberg, S. Lloyd, and D. Englund, "Bosonic transport simulations in a large-scale programmable nanophotonic processor," arXiv: 1507.03406 (2015).
23. J. Wang, A. Santamato, P. Jiang, D. Bonneau, E. Engin, J. W. Silverstone, M. Lermer, J. Beetz, M. Kamp, S. Höfling, M. G. Tanner, C. M. Natarajan, R. H. Hadfield, S. N. Dorenbos, V. Zwiller, J. L. O'Brien, and M. G. Thompson, "Gallium arsenide (GaAs) quantum photonic waveguide circuits," Opt. Commun. **327**, 49–55 (2014).
24. R. Osellame, G. Cerullo, and R. Ramponi, *Femtosecond Laser Micromachining Photonic and Microfluidic Devices in Transparent Materials* (Springer, 2012).
25. K. K. Mehta, C. D. Bruzewicz, R. McConnell, R. J. Ram, J. M. Sage, and J. Chiaverini, "Integrated optical addressing of an ion qubit," Nat. Nanotechnol. **11**(12), 1066–1070 (2016).
26. K. R. Brown, J. Kim, and C. Monroe, "Co-designing a scalable quantum computer with trapped atomic ions," arXiv:1602.02840v1.
27. S. Richter, C. Miese, S. Döring, F. Zimmermann, M. J. Withford, A. Tünnermann, and S. Nolte, "Laser induced nanogratings beyond fused silica – periodic nanostructures in borosilicate glassess and ULE^{TM}," Opt. Mater. Express **3**(8), 1161–1166 (2013).
28. L. A. Fernandes, J. R. Grenier, P. R. Herman, J. S. Aitchison, and P. V. S. Marques, "Femtosecond laser writing of waveguide retarders in fused silica for polarization control in optical circuits," Opt. Express **19**(19), 18294–18301 (2011).
29. R. Heilmann, M. Gräfe, S. Nolte, and A. Szameit, "Arbitrary photonic wave plate operations on chip: realizing Hadamard, Pauli-X, and rotation gates for polarisation qubits," Sci. Rep. **4**, 4118 (2014).
30. L. A. Fernandes, J. R. Grenier, P. R. Herman, J. S. Aitchison, and P. V. S. Marques, "Femtosecond laser fabrication of birefringent directional couplers as polarization beam splitters in fused silica," Opt. Express **19**(13), 11992–11999 (2011).
31. K. R. Motes, J. P. Dowling, and P. P. Rohde, "Spontaneous parametric down-conversion photon sources are scalable in the asymptotic limit for boson sampling," Phys. Rev. A **88**(6), 063822 (2013).
32. P. J. Mosley, J. S. Lundeen, B. J. Smith, P. Wasylczyk, A. B. U'Ren, C. Silberhorn, and I. A. Walmsley, "Heralded generation of ultrafast single photons in pure quantum States," Phys. Rev. Lett. **100**(13), 133601 (2008).
33. K. Hirao and K. Miura, "Writing waveguides and gratings in silica and related materials by a femtosecond laser," J. Non-Cryst. Solids **239**(1–3), 91–95 (1998).
34. J. Liu, Z. Zhang, C. Flueraru, X. Liu, S. Chang, and C. P. Grover, "Waveguide shaping and writing in fused silica using a femtosecond laser," IEEE J. Sel. Top. Quantum Electron. **10**(1), 169–173 (2004).
35. L. Shah, A. Arai, S. Eaton, and P. Herman, "Waveguide writing in fused silica with a femtosecond fiber laser at 522 nm and 1 MHz repetition rate," Opt. Express **13**(6), 1999–2006 (2005).
36. Y. Nasu, M. Kohtoku, and Y. Hibino, "Low-loss waveguides written with a femtosecond laser for flexible interconnection in a planar light-wave circuit," Opt. Lett. **30**(7), 723–725 (2005).
37. S. M. Eaton, M. L. Ng, R. Osellame, and P. R. Herman, "High refractive index contrast in fused silica waveguides by tightly focused, high-repetition rate femtosecond laser," J. Non-Cryst. Solids **357**(11–13), 2387–2391 (2011).
38. H. Huang, L.-M. Yang, and J. Liu, "Femtosecond fiber laser direct writing of optical waveguide in glasses," Proc. SPIE **8164**, 81640B (2011).
39. J. Tang, C. Chen, T. Chang, S. Wang, L. Chau, and W. Wu, "Fabrication and characterization of a fused silica-based optical waveguide with femtosecond fiber laser pulses," Microsyst. Technol. **18**(11), 1815–1821 (2012).

Optics EXPRESS

40. S. M. Eaton, W.-J. Chen, H. Zhang, R. Iyer, J. Li, M. L. Ng, S. Ho, J. S. Aitchison, and P. R. Herman, "Spectral loss characterization of femtosecond laser written waveguides in glass with application to demultiplexing of 1300 and 1550 nm wavelengths," J. Lightwave Technol. **27**(9), 1079–1085 (2009).
41. Y. Shimotsuma, P. G. Kazansky, J. Qiu, and K. Hirao, "Self-organized nanogratings in glass irradiated by ultrashort light pulses," Phys. Rev. Lett. **91**(24), 247405 (2003).
42. L. Shah, A. Arai, S. Eaton, and P. Herman, "Waveguide writing in fused silica with a femtosecond fiber laser at 522 nm and 1 MHz repetition rate," Opt. Express **13**(6), 1999–2006 (2005).
43. R. Hui and M. O'Sullivan, Fiber Optic Measurement Techniques, (Elsevier Academic Press, 2009).
44. A. Jesacher, P. S. Salter, and M. J. Booth, "Refractive index profiling of direct laser written waveguides: tomographic phase imagine," Opt. Mater. Express **3**(9), 1223–1232 (2013).
45. L. B. Jeunhomme, *Single-Mode Fiber Optics Principles and Applications* (Marcel Dekker, Inc 1990).
46. Y. Ohtsuka, T. Ando, Y. Imai, and M. Imai, "Modal birefringence measurements of polarization-maintaining single-mode fibers without and with stretching by optical heterodyne interferometry," J. Lightwave Technol. **5**(4), 602–607 (1987).
47. M. Müller, J. Squier, K. R. Wilson, and G. J. Brakenhoff, "3D microscopy of transparent objects using third-harmonic generation," J. Microsc. **191**(3), 266–274 (1998).
48. A. Jesacher, A. Thayil, K. Grieve, D. Débarre, T. Watanabe, T. Wilson, S. Srinivas, and M. Booth, "Adaptive harmonic generation microscopy of mammalian embryos," Opt. Lett. **34**(20), 3154–3156 (2009).
49. G. D. Marshall, A. Jesacher, A. Thayil, M. J. Withford, and M. Booth, "Three-dimensional imaging of direct-written photonic structures," Opt. Lett. **36**(5), 695–697 (2011).
50. G. Cerullo, R. Osellame, S. Taccheo, M. Marangoni, D. Polli, R. Ramponi, P. Laporta, and S. De Silvestri, "Femtosecond micromachining of symmetric waveguides at 1.5 microm by astigmatic beam focusing," Opt. Lett. **27**(21), 1938–1940 (2002).
51. Y. Cheng, K. Sugioka, K. Midorikawa, M. Masuda, K. Toyoda, M. Kawachi, and K. Shihoyama, "Control of the cross-sectional shape of a hollow microchannel embedded in photostructurable glass by use of a femtosecond laser," Opt. Lett. **28**(1), 55–57 (2003).
52. M. Ams, G. Marshall, D. Spence, and M. Withford, "Slit beam shaping method for femtosecond laser direct-write fabrication of symmetric waveguides in bulk glasses," Opt. Express **13**(15), 5676–5681 (2005).
53. F. He, H. Xu, Y. Cheng, J. Ni, H. Xiong, Z. Xu, K. Sugioka, and K. Midorikawa, "Fabrication of microfluidic channels with a circular cross section using spatiotemporally focused femtosecond laser pulses," Opt. Lett. **35**(7), 1106–1108 (2010).
54. R. Osellame, N. Chiodo, G. della Valle, S. Taccheo, R. Ramponi, G. Cerullo, A. Killi, U. Morgner, M. Lederer, and D. Kopf, "Optical waveguide writing with a diode-pumped femtosecond oscillator," Opt. Lett. **29**(16), 1900–1902 (2004).
55. V. R. Bhardwaj, P. B. Corkum, D. M. Rayner, C. Hnatovsky, E. Simova, and R. S. Taylor, "Stress in femtosecond-laser-written waveguides in fused silica," Opt. Lett. **29**(12), 1312–1314 (2004).
56. L. A. Fernandes, J. R. Grenier, P. R. Herman, J. S. Aitchison, and P. V. S. Marques, "Stress induced birefringence tuning in femtosecond laser fabricated waveguides in fused silica," Opt. Express **20**(22), 24103–24114 (2012).
57. G. Cheng, K. Mishchik, C. Mauclair, E. Audouard, and R. Stoian, "Ultrafast laser photoinscription of polarization sensitive devices in bulk silica glass," Opt. Express **17**(12), 9515–9525 (2009).
58. R. S. Taylor, E. Simova, and C. Hnatovsky, "Creation of chiral structures inside fused silica glass," Opt. Lett. **33**(12), 1312–1314 (2008).
59. W. Yang, E. Bricchi, P. G. Kazansky, J. Bovatsek, and A. Y. Arai, "Self-assembled periodic sub-wavelength structures by femtosecond laser direct writing," Opt. Express **14**(21), 10117–10124 (2006).
60. Y. Fu, T. Ye, W. Tang, and T. Chu, "Efficient adiabatic silicon-on-insulator waveguide taper," Photonics Res. **2**(3), A41–A44 (2014).

1. Introduction

Photonic integrated circuits (PICs) that are employed in quantum information processing (QIP) can be categorized into two groups according to their fabrication techniques: direct written waveguide circuits [1–17] and waveguide circuits fabricated with complementary metal-oxide-semiconductor (CMOS) processing technology [18–23]. Although waveguide circuits fabricated with CMOS processing techniques can take advantage of the well-developed CMOS manufacture facilities and processes, they require complex fabrication processes which involve patterning, etching and so on. On the contrary, direct writing basically is a single-step-process fabrication technique. Direct written waveguide circuits can be further sub-grouped into ultrashort-pulsed laser written (UPLW) waveguide circuits [1–13] and UV-written waveguide circuits [14–17]. Unlike the UV writing technique, which is limited to planar circuits with doped silica, UPLW is not only an intrinsically three-dimensional fabrication technique, but also flexible with many transparent materials. But up

Optics EXPRESS

to now, a drawback of UPLW waveguide circuits is that the propagation losses have been typically higher than their CMOS-process based counterparts [24]. Loss is one of the key impediments to future scaling of UPLW waveguide circuits for photon-based QIPs [17]. Along with losses, the polarization dependencies of waveguides are also critical for many photon-based QIPs that involve interference [14] or rely on photon polarization [3]. The polarization states of a photon can be manipulated through integrated waveplates and polarization beam splitters (PBSs), however the waveguides are required to be polarization-independent to maintain the fidelity of the information being processed [3].

Some of the reported UPLW waveguide circuits for photon-based QIPs were written in fused silica [1, 4, 8–10] and some others were written in other glasses like borosilicate glass [2, 3, 5–7, 11–13]. Nevertheless, despite the relative difficulty of writing waveguides in pure fused silica than in other glasses that have lower band gaps and softening points, like borosilicate glass, currently we still regard pure fused silica as a promising substrate material for UPLW waveguide circuits for photon-based QIPs, especially when we are aiming at future practical applications of the UPLW waveguide circuits based QIPs. The reasons for this are: (i) pure fused silica has higher physical and chemical stabilities; (ii) and pure fused silica shows high transmittance over a broad spectral range (this could be a significant advantage of pure fused silica UPLW waveguide circuits for ion-trap-based QIP that requires UPLW waveguide circuits also to work at around 400 nm wavelength [25, 26]); (iii) due to the nanograting-induced birefringence being stronger in fused silica than in other glasses [27], it is relatively easier to fabricate integrated waveplates [28, 29], PBSs [30] and other birefringence based devices in fused silica.

Photon sources based on spontaneous parametric down-conversion (SPDC) are widely used in photon-based QIPs [31]. The work presented here focuses on single-mode laser written waveguides at wavelength of around 800 nm, based on the wavelength of the SPDC photon source [15–17, 32] of our intended QIP applications.

Straight waveguides are the fundamental building blocks of the UPLW waveguide circuits. Moreover, the writing parameters of straight waveguides serve as the basis for the writing parameters of other integrated components in UPLW waveguide circuits. Several groups have studied the femtosecond laser written straight waveguides in fused silica [33–39]. In term of propagation loss, to date the best reliable result was 0.12 dB/cm at 1550 nm wavelength, which was written with a 1 kHz repetition rate femtosecond laser through multiple scanning and measured through accurate cut-back approach [36]. Considering that Rayleigh scattering is a major loss mechanism [40], the propagation loss of a waveguide at 1550 nm wavelength tends to be significantly lower than that at around 800 nm. Among those reported waveguides, polarization dependency of the waveguides has not been extensively investigated, although Nasu *et al.* have measured the polarization-dependent loss of the written waveguide [36].

In this work, we first investigated the relationship between the writing parameters and the properties of the straight waveguides written in pure fused silica, in term of propagation loss, insertion loss coupled from a single-mode fibre and polarization dependency. Then we demonstrated a way to fabricate waveguides with properties that vary along their length to provide not only low total insertion losses but also low polarization dependency at the same time. In the meantime based on the results of this investigation, several useful revelations were disclosed. It is also worth to mention that in this work only the single-scan writing approach was used, since the multiple-scan is not only intrinsically less efficient but also in principle suffers from higher scattering loss due to the non-uniformity introduced by the separations of the different scanning passes.

2. Waveguide fabrication and characterization

Waveguides were written inside fused silica (Schott Lithosil Q0) with a tightly focused 1 MHz repetition rate, 514 nm wavelength, 170 fs pulse duration laser which was the second

Optics EXPRESS

harmonic of a regenerative amplified Yb:KGW laser (Light Conversion Pharos SP-06-1000-pp). Before being focused 117 μm below the top surface of the glass with a 0.5 NA objective lens, the power of the writing beam was controlled with a motorized rotating half waveplate together with a PBS. The writing beam was circularly polarized to suppress the creation of nanogratings [41]. The fused silica chip, which was fixed on a three axis air bearing stage (Aerotech ABL10100L/ABL10100L/ANT95-3-V), was transversely scanned relative to the focus to inscribe waveguides.

The laser pulse energy and the scanning speed were varied in order to determine the optimum writing parameters. We combine these parameters into the representative net fluence (RNF). Similar to the definition of net fluence in reference [42], here the writing RNF is defined as:

$$RNF = \frac{4RE_p}{\pi V_s D}. \quad (1)$$

where R is the repetition rate, E_p is the pulse energy measured at sample surface, V_s is the scanning speed of the translation stage, D is the diameter of the focus spot of writing beam in air.

2.1 The relationship between loss and representative net fluence

With our fabrication system and settings, when the scanning speed was set at 0.01 mm/s, the threshold of laser-induced refractive index change in fused silica was at a RNF of around 3.2 mJ/μm^2. The upper limit of RNF, at which the written waveguides still appeared homogeneous under a differential interference contrast (DIC) microscope, was around 3.8 mJ/μm^2. Within this RNF range, waveguides were written in a fused silica chip with RNFs of 3.25, 3.31, 3.38, 3.47, 3.55, 3.64 and 3.69 mJ/μm^2 respectively, in which pulse energy was varied from 27 nano-joules to 30 nano-joules and the scanning speed was fixed at 0.01 mm/s. The lengths of the original chip and those of all the written waveguides were 40 mm.

To measure the insertion losses and near-field mode profiles of the written waveguides, a 777 nm wavelength (measured with Ocean Optics USB2000 spectrometer) linearly polarized laser beam was coupled into each waveguide through butt-coupling with a polarization-maintaining (PM) fibre (Thorlabs P1-630PM-FC-5); the output from a waveguide was imaged onto a CCD camera through an objective lens and a tube lens. A photodiode power sensor was used to measure the power of the output beam from a waveguide. To further reduce the almost negligible influence of the unguided light after the objective lens, when the output power was measured, the power sensor was placed 220 mm behind the objective lens and an iris was inserted before the power sensor.

All the written waveguides were single mode at 777 nm. The propagation losses were determined with the cutback approach [43]. Before and after cutting, the lengths of the polished chip were 38.8 mm and 14.2 mm respectively. The relationships between insertion losses of the waveguides and the corresponding writing RNFs before and after cutting are shown in Fig. 1. Each insertion loss was measured multiple times with coupling laser beam in vertical polarization (VP) and in horizontal polarization (HP) respectively. The horizontal solid and dashed lines on the left part of Fig. 1 and following figures will be explained in subsection 2.3; they are included here and in following figures for later direct comparisons. The error bars in Fig. 1 represented the measurement uncertainties of insertion losses due to the couplings between the PM fibre and the waveguides. The error bars were multiplied with a factor of 4 in Fig. 1 for their visibility. In this report, all the measurements were performed without using any index-matching fluid and all the error bars represented peak-to-peak error values.

Optics EXPRESS

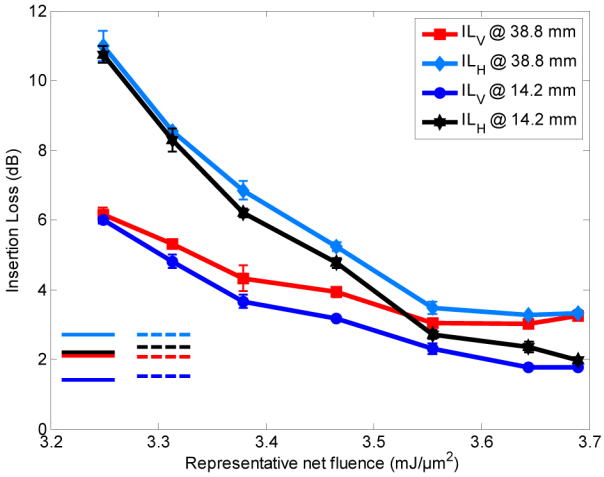

Fig. 1. Measured insertion losses in vertical and horizontal polarizations at waveguide lengths of 38.8 mm and 14.2 mm respectively; The horizontal solid and dashed lines in the lower left part of this figure and following figures represent results that will be explained in subsection 2.3; they are included here and in following figures for later direct comparisons.

Insertion losses measured with the VP beam (IL_V) were lower than those measured with the HP beam (IL_H). And the difference between IL_V and IL_H decreased along with the increase in writing RNF. The reason for those polarization related phenomena will be explained in next subsection. In all cases, the insertion loss decreased with increasing RNF. This was due to the fact that higher RNF gave rise to higher refractive index change, which resulted in a decrease in the coupling loss with the PM fibre. The refractive index changes were measured with a home-built quantitative phase microscope, with which the averaged refractive index profile across the waveguide cross-section shown in Fig. 2 was obtained through solving the transport of intensity equation [44]. The refractive index change, averaged across the waveguide, was calculated by dividing the measured optical path length by the depth of the whole waveguide structure (including guiding region and negative refractive index change region); the depth of the whole waveguide structure was measured with an adaptive third-harmonic generation (THG) microscope.

Optics EXPRESS

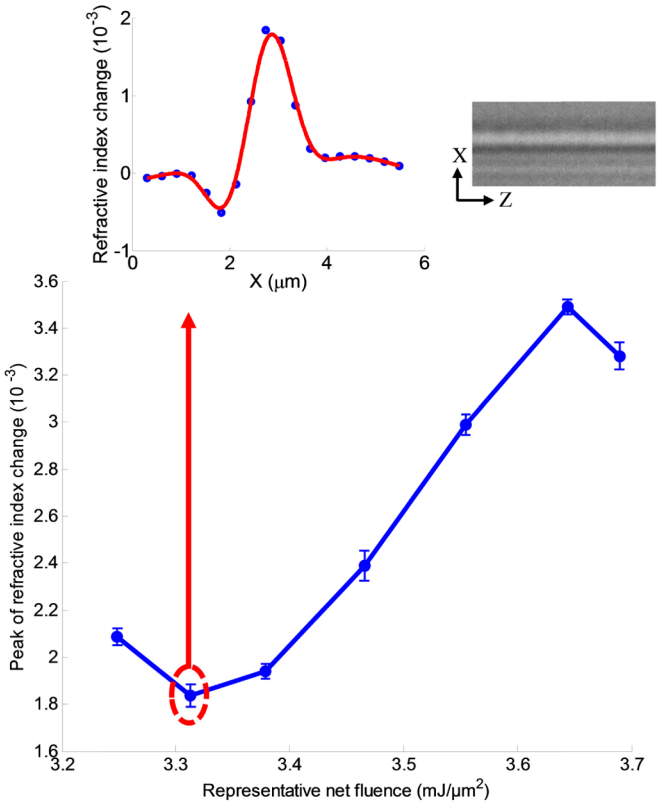

Fig. 2. Peak of the averaged refractive index profile for waveguides written with different RNFs; as an example, the measured refractive index change profile and the transmission microscope image (along the writing direction Z) of the waveguide written with RNF of 3.31 mJ/μm^2 are shown in in the upper part of the figure.

Based on the measured insertion losses before and after cutting back, the propagation losses were calculated, as shown in Fig. 3. Both the propagation loss (PL_V) at VP and the propagation loss (PL_H) at HP were increasing along with the writing RNF. The waveguide written with 3.25 mJ/μm^2, which was just above the 3.2 mJ/μm^2 threshold for refractive index change, showed average propagation losses of 0.06 dB/cm and 0.1 dB/cm at wavelength of 777 nm for VP and HP respectively.

Propagation loss normally includes absorption, scattering and radiation loss [24]. Based on the relationship between refractive index change and the writing RNF that is shown in Fig. 2, the radiation loss should decrease along with an increase in writing RNF, since greater refractive index change will result in better confinement of the light propagating in the waveguide. Therefore, assuming that the absorption properties of the fused silica are not significantly affected within the RNF range, from Fig. 3 following conclusion could be drawn: within the RNF range, along with increase of writing RNF, scattering played an increasingly dominant role in the propagation loss. These phenomena were also disclosed in reference [40] for waveguides in in borosilicate glass, as measured through spectral loss characterization.

Optics EXPRESS

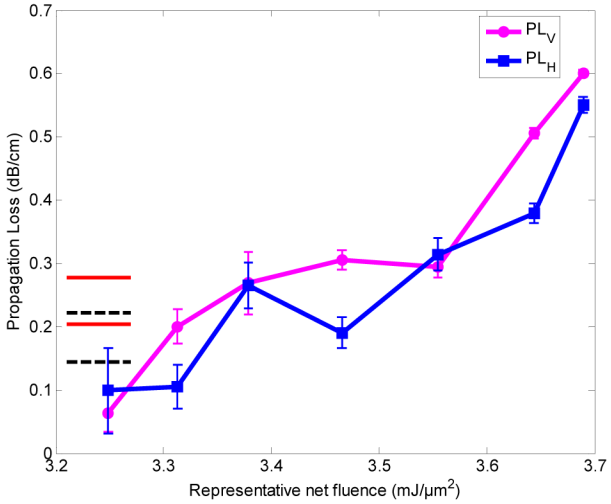

Fig. 3. The relationship between measured propagation losses of the waveguides and their writing RNFs. The horizontal solid and dashed lines in the lower left part of this figure are explained in subsection 2.3

2.2 The relationship between polarization dependence and writing representative net fluence

From the measured insertion losses in Fig. 1, the polarization dependence of each waveguide, which was represented by the difference between IL_H and IL_V, was calculated and shown in Fig. 4. Clearly the polarization dependence decreased with increasing writing RNF, from around 4.8 dB at 3.25 mJ/μm^2 to about 0.15 dB at 3.69 mJ/μm^2. In the subsequent discussion we explain the reason behind this trend according to the combined effect between the so-called 'shape birefringence' [45] and stress-induced birefringence; the combined overall birefringence is usually known as modal birefringence [46]. Shape birefringence means that the effective refractive indices of the waveguides are different for VP and HP, which is due to the noncircular cross-sections of the waveguides.

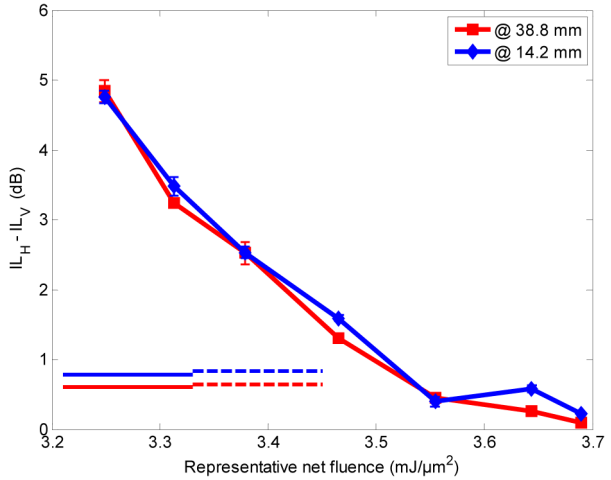

Fig. 4. The polarization dependence (IL_H-IL_V) of waveguides written with different RNFs. The horizontal solid and dashed lines in the lower left part of this figure are explained in subsection 2.3

Optics EXPRESS

An adaptive THG microscope was used to probe the cross-section profiles of the written waveguides, since the third harmonic signals are sensitive to changes in refractive index or the third-order nonlinear susceptibility ($\chi^{(3)}$) and thus reveal the shape of the laser modified regions [47–49]. All the written waveguides were found to be elongated along the propagation direction of the writing beam, since they were written without any beam shaping [50–53]. As an example, the THG images of waveguides written with 3.25 mJ/μm^2 and 3.69 mJ/μm^2 are shown in Fig. 5; the insets are their corresponding optical transmission microscope images of the end facets. The lower part of each laser inscribed structure formed its light guiding region, as indicated with dashed rectangles in Fig. 5. A detailed explanation of the THG images will be given in a following report; the features visible above the guiding region are believed to be part of the low index non-guiding feature of the laser written structure. Here it is worth noting that when imaging laser-written waveguides, a stronger third harmonic signal correlates with a greater gradient of the refractive index change.

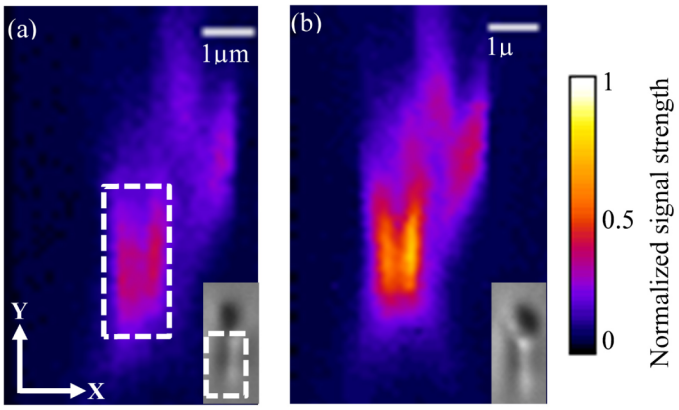

Fig. 5. Adaptive THG microscope images (in false color) and their corresponding optical transmission microscope images (insets) of waveguides written with 3.25 mJ/μm^2 (a) and with 3.69 mJ/μm^2 (b); in (a), the light guiding region is indicated with dashed rectangles, the non-guiding upper part is the region with negative refractive index change.

Provided that the output coupling losses were approximately zero during the insertion loss measurements (this is reasonable, since an objective lens was employed for output coupling), the difference between IL_H and IL_V is given by:

$$IL_H - IL_V = CL_H - CL_V + (PL_H - PL_V)L. \quad (2)$$

where CL_H and CL_V are the coupling loss from the PM fibre at HP and VP respectively; L is the length of a waveguide in centimeters; IL_H, IL_V, CL_H and CL_V are in dB; propagation losses PL_H and PL_V are in dB/cm. From Fig. 4 we can see that the difference between polarization dependences (IL_H - IL_V) at before-cut-back (38.8 mm) and after-cut-back (14.2 mm) is insignificant for each waveguide, which means that the dominant reason for the waveguide polarization dependence is the difference of coupling losses in two polarization directions (HP and VP) (CL_H - CL_V in Eq. (2)), not the difference between propagation losses at HP and VP ((PL_H - PL_V)L). This was also confirmed by simulation, which was not shown here, based on mode matching [54] between a waveguide and the PM fibre with their recorded near field mode profiles.

For a waveguide, shape birefringence will result in unequal coupling losses in different polarizations; but this was not the only reason behind the trend shown in Fig. 4. This was due to the fact that the cross sectional aspect ratio of waveguide (i.e. the guiding region) did not increase along with writing RNF, as an example shown in Fig. 5, which indicated that shape birefringence also should not have decreased. But the value of IL_H - IL_V decreased along with

Optics EXPRESS

increasing writing RNF in Fig. 4. This contradiction implied other kind(s) of birefringence must have been present in the written waveguides.

Aside from shape birefringence, there are two other known mechanisms of laser-induced birefringence in fused silica: stress-induced birefringence [55, 56] and birefringence induced by nanograting structures [41, 57]. Both the use in the writing beam of circular polarization [58] and of repetition rates over 500 kHz [59] have previously been shown to avoid nanograting structures in fused silica; and during this work, all the waveguides were written with a circularly polarized laser beam at repetition rate of 1 MHz. Therefore it was reasonable for us to assume that there was no nanograting-induced birefringence, and that shape birefringence and stress-induced birefringence were dominant. From the polarization dependency trend shown in Fig. 4, two following conclusions were drawn: (i) the slow axes of the stress-induced birefringence and the shape birefringence did not overlap, since along with the increase in writing RNF the shape birefringence and stress-induced one tended to cancel each other out; (ii) the stress-induced birefringence increased with the writing RNF, since the shape birefringence did not decrease but the overall polarization dependency did.

Therefore, more importantly, it was revealed that through balancing the counter-effects between shape birefringence and stress-introduced one, waveguides with concurrent low polarization-dependence and low loss can be fabricated, which are important for many photon-based QIP applications [14]. The stress-induced birefringence, which always appears, can be adjusted with the writing RNF. The shape birefringence depends on the cross-section of the waveguides, which can be controlled with shaping [50–53] of the writing beam to get certain non-circular cross-section of waveguides to cancel out the ever-appearing stress-induced birefringence. Theoretically, nanograting-induced birefringence also can be employed to cancel out the stress-induced birefringence to attain polarization-dependency-free waveguides, but up to now nanograting-induced birefringence is less controllable than beam shaping. In addition to the uncontrollability, nanograting-induced birefringence is also sensitive to the wavelength of the propagating beam [57].

As indicated in Fig. 4, it is possible to fabricate non-polarization-dependent waveguides without employing beam shaping techniques, but at the cost of propagation loss, since as revealed in section 2.1, scattering, a dominant factor for the propagation loss, is dependent on the writing RNF. A straightforward solution towards low-propagation-loss and low-polarization-dependence waveguides in fused silica is to write waveguides with low RNF, using certain non-circular waveguide cross-sections with the help of beam shaping, and suppressing nanogratings at the same time. But there are three drawbacks for this straightforward solution: (i) the additional cost and complexity that will be incurred by a beam shaping unit; (ii) curved waveguides written with low RNF will suffer from high bend loss; (iii) due to the poor ability of confinement, waveguides written with low RNF have wide mode profiles which will result in high coupling losses with the commonly used single mode fibres. For example, the waveguide written with 3.25 mJ/μm^2 RNF had a mode field diameter (MFD) of around three times of that of the coupling PM fibre in horizontal polarization. The multiple-scan writing technique can be used to increase the waveguide width and decrease the coupling losses, but the multiple-scan will intrinsically increase the propagation losses. To this end, a simple and better solution will be presented in next subsection. But before that, an investigation on stress-induced birefringence only was performed to further confirm our understanding of its relationship with writing RNF.

Optics EXPRESS

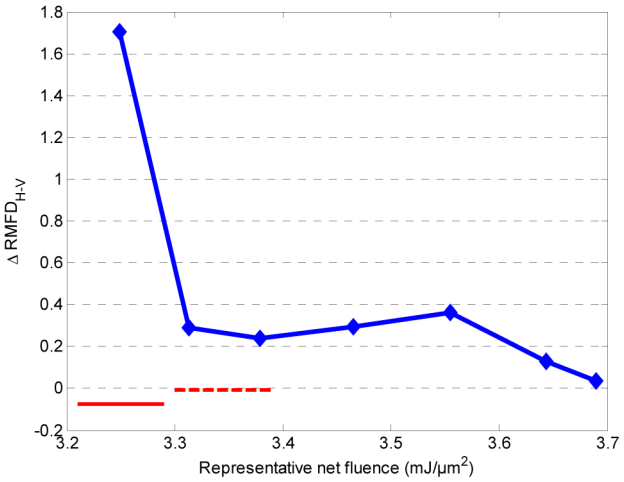

Fig. 6. The difference between normalised mode field diameters of waveguides in horizontal polarization ($RMFD_H$) and vertical polarization ($RMFD_V$); $RMFD_H$ and $RMFD_V$ were normalised to the mode field diameters of the PM fibre in corresponding polarization. The horizontal solid and dashed lines in the lower left part of this figure are explained in subsection 2.3

Complete decoupling of the stress-induced birefringence from the shape birefringence is not straightforward. However, based on the aforementioned investigations, we knew that the slow axes of the shape birefringence of all written waveguides were along Y direction in Fig. 5 (a), which was vertical polarization direction. The reason for that was following: the MFDs of the all waveguides in vertical polarization always were smaller than those in other polarization directions like the horizontal one, as an example, the difference between normalised mode field diameters of waveguides in horizontal polarization ($RMFD_H$) and vertical polarization ($RMFD_V$) is shown in Fig. 6, where $RMFD_H$ and $RMFD_V$ were normalised to the mode field diameters of the PM fibre in the corresponding polarization.This indicated that the effective refractive indices of the waveguides were greater in vertical polarization direction than in other polarization directions. As indicated in Fig. 6, the disparity of effective refractive indices at two polarization directions was more pronounced for waveguides written with lower RNF where stress-induced birefringence was lower [55]. As concluded previously, the slow axes of shape and stress-induced birefringence did not overlap. Therefore to single out the stress-induced birefringence, a vertical polarized laser beam from a PM fibre was coupled into each waveguide and the change of state of polarization (SOP) of the each waveguide between input and output was measured with a polarimeter (Polarization Analyzer SK010PA-VIS, Schäfter + Kirchhoff GmbH). However due to the weakness of the stress-induced birefringence and the limited length of waveguides, among all the measured SOP parameters, only the change of the azimuth angle $\Delta\Phi$ was repeatable and reliable during the investigation. $\Delta\Phi$ was the change of azimuth angle of the semi-major axis of the polarization ellipse, from input beam to output beam. The measured $\Delta\Phi$ for each waveguide is shown in Fig. 7. From that figure, the stress-induced birefringence was confirmed to increase with writing RNF (pulse energy), which was also proved in reference [55] with different measurement approach and filtering out the shape birefringence with beam shaping. Accordingly it was further confirmed that the slow axes of shape and stress-induced birefringence did not overlap.

Optics EXPRESS

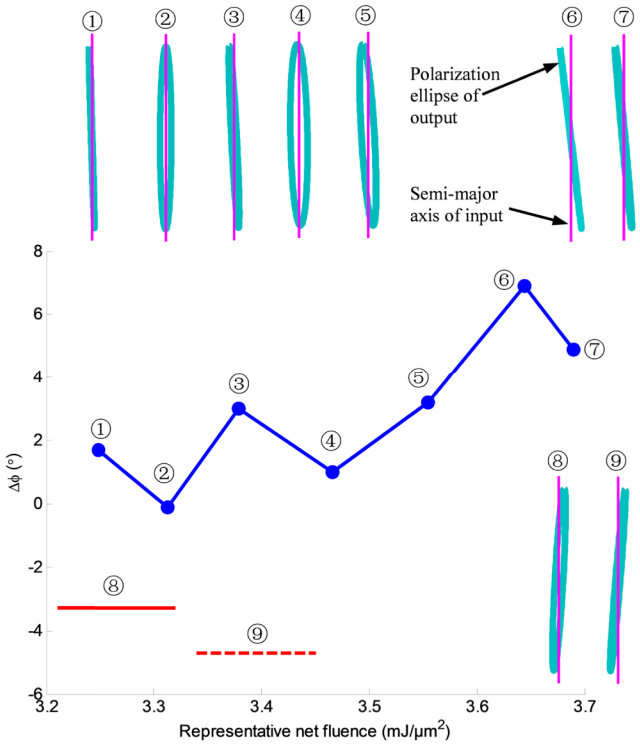

Fig. 7. Measured ΔΦ for waveguides written with different RNFs; insets are the measured relative polarization ellipses of the output beams from corresponding waveguides, with respect to the semi-major axis of the polarization ellipse of the input beam. The results labeled 8 and 9 are explained in subsection 2.3.

2.3 Fabrication of hybrid waveguides with low insertion loss and low polarization dependence

Based on the results of the previous sections, an approach to fabricate waveguides with low insertion loss and low polarization dependence was demonstrated as a proof-of-principle. This approach was to fabricate a hybrid waveguide (HW) making use the beneficial properties of waveguide structure written with low RNF and the fact that the mode profile of a waveguide can be adjusted with writing RNF. Figure 8(a) shows, as an example, an adiabatic mode converter (AMC) was fabricated at one end of the HW that needed to be coupled with another waveguide – in this case a PM fibre. The rest of the waveguide was written at low RNF. The AMC converted the output modes of the input waveguide (the PM fibre in this case) to the modes of the waveguide written with low RNF, in all polarization directions. In this way the coupling loss from coupled waveguide was reduced and at the same time the propagation loss and polarization dependence of the whole HW were reduced thanks to the properties of the waveguide structure written with low RNF and the function of AMC. Since the birefringence of the waveguide written with low RNF was mainly shape birefringence, the disparity of its coupling losses between two polarization directions could be reduced with the AMC and the polarization dependence of the whole HW could be reduced as a result. By virtue of femtosecond laser direct writing, the AMC could be easily fabricated by varying the power or the number of the pulses of the writing laser during the single scan of the HW, which is in contrast to the complexities of design and fabrication of mode converter in a silicon-on-insulator chip [60].

Optics EXPRESS

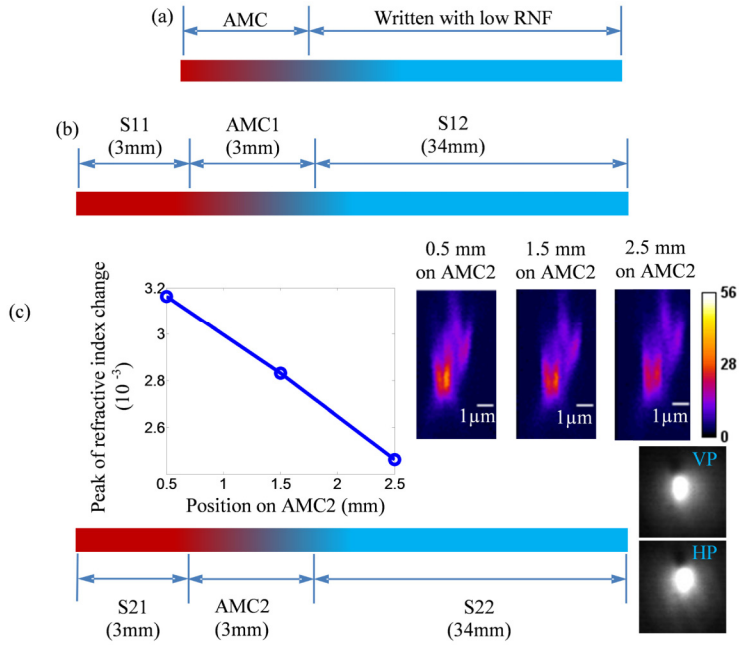

Fig. 8. (a) Schematic of the proposed hybrid waveguide; (b) design of HW1; (c) design of HW2 (lower), the recoded mode profiles of the fabricated HW2 (right), measured peak of refractive index change at three positions on AMC2 (upper left) and the THG microscopy cross-section images (upper right, in false colors) of AMC2 at corresponding positions.

To test the principle of this hybrid waveguide, two hybrid waveguides, HW1 and HW2, were fabricated. The designs of those two HWs are schematically illustrated in Fig. 8(b) and (c). Section S11 in HW1 and section S21 in HW2 were written with RNF of 3.69 mJ/μm^2; Section S12 and section S22 were written with RNF 3.31 mJ/μm^2 and 3.25 mJ/μm^2 respectively; AMC1 and AMC2 were fabricated by gradually lowering the RNF (only the pulse energy was lowered here) from 3.69 mJ/μm^2 to 3.31 mJ/μm^2 and 3.25 mJ/μm^2 respectively during scanning of the writing beam. It is worth mentioning that the 3 mm length of AMC1 and AMC2 was selected empirically only to prove the principle. The adiabaticities and other properties of AMC1 and AMC2 are subject to further study. Section S11 and S21 were used as lead-in regions that were fabricated to protect AMC1 and AMC2 during polishing of the chips. HW1 and HW2, together with the normal waveguides described in previous subsection 2.1 and 2.2, were fabricated on the same chip and went through the same investigation. As an example, the recorded output mode profiles of HW2 in VP and HP are shown in Fig. 8(c). The evolution of refractive index change along AMC2 can be sensed from the measured refractive index change at three positions, upper left on Fig. 8(c), and the corresponding THG microscope cross-section images, upper right on Fig. 8(c). The performances (measured mean values) of HW1 and HW2 were summarized in Table 1. To enable direct comparison of the performance of HW1 and HW2 with those waveguides written with constant RNFs, the relevant values of HW1 and HW2 were marked in previous Fig. 1, 3, 4, 6 and 7; the values of HW1 were marked with horizontal solid lines and those of HW2 were marked with dashed lines.

Clearly, in comparison with those waveguides written with constant RNFs, HW1 and HW2 had low insertion losses, low effective propagation losses and low polarization dependencies at the same time. The longer the hybrid waveguides are, the more pronounced their advantages will be, since their effective propagation losses will be more close to the waveguides written with low RNFs and at the same time their polarization dependencies are

Optics EXPRESS

predominantly decided by the AMCs and have insignificant dependencies on the lengths of HWs.

Table 1. Summary of the performances (measured mean values) of HW1 and HW2.

	IL_V (dB)		IL_H (dB)		PL_V (dB/cm)	PL_H (dB/cm)	IL_H - IL_V (dB)		ΔΦ (°)	RMFD[a]	
	@ 38.8 mm	@ 14.2 mm	@ 38.8 mm	@ 14.2 mm			@ 38.8 mm	@ 14.2 mm	@ 14.2 mm	VP	HP
HW1	2.11	1.43	2.71	2.21	0.28	0.20	0.60	0.78	–3.3	1.36	1.35
HW2	2.06	1.52	2.70	2.35	0.22	0.14	0.64	0.83	–4.7	1.42	1.42

[a]RMFD: the ratio between MFDs of waveguides and the those of the PM fibre in VP and HP.

Meanwhile, it was noticeable that the signs of the $\Delta RMFD_{H-V}$ and the ΔΦ values of HW1 and HW2, as shown in Fig. 6, Table 1 and Fig. 7 respectively, were opposite to those of the waveguides written with constant RNFs. It indicated that the values of IL_H - IL_V for AMCs were negative, which were opposite to the positive values of IL_H - IL_V for waveguides written with constant RNFs. It meant that the AMCs behaved differently from waveguides written with constant RNFs in term of insertion losses at different polarizations. The reason behind that requires further study. However this phenomenon implied another possible way to fabricate polarization-dependency-free and low loss waveguides through design of a suitable AMC, along with the aforementioned approach through balancing the shape birefringence and stress-induced birefringence.

3. Conclusion

An approach to fabrication of waveguides with not only low propagation and insertion losses but also low polarization dependence at the same time was demonstrated as a proof-of-principle. Although shown here with straight waveguides, it could also be straightforwardly extended to curved waveguides, noting that to reduce bend losses at curved regions, high writing RNF normally should be used. Furthermore, a way to fabricate low loss waveguides without polarization dependence or with designed polarization dependency (i.e. birefringence) was suggested, in which the modal birefringence was controlled through manipulating the shape birefringence under suppression of nanogratings. This could be achieved, since once the writing parameters like scanning speed and pulse energy were chosen for low propagation loss, the stress-induced birefringence, which would also be decided by the writing parameters, would be fixed; but the shape birefringence could still be manipulated by beam shaping of the writing beam. Moreover following four points were also revealed or confirmed through different methods: (i) scattering as the dominant factor for propagation loss in laser written waveguides in fused silica was confirmed; the same finding was previously revealed in borosilicate glass through spectral loss characterization [40]; (ii) the polarization dependence of laser written waveguides in fused silica is predominantly due to the difference of coupling losses in different polarization directions, which results from the different effective refractive indices in different polarization directions; (iii) the slow axes of shape birefringence and stress-induced birefringence did not overlap in pure fused silica with normal transverse laser writing approach and without beam shaping; (iv) if the waveguides were not annealed to release stress as shown in reference [55], counter-intuitively, certain non-circular waveguide cross-sections were required to fabricate waveguides with simultaneous low loss and free of polarization dependence.

Funding

UK EPSRC (EP/M013243/1, EP/K034480/1).

Optics EXPRESS

Acknowledgments

This publication was supported by the Oxford RCUK Open Access Block Grant and accordingly underlying research materials are available upon request to the authors.